Supplementary Information

Macrocycle supported dinuclear lanthanide complexes with different *β*-diketonate co-ligands displaying zero field single-molecule magnetic behaviour

Kuheli Pramanik,[a,b] Yu-Chen Sun,[c] Paula Brandão,[d] Narayan Ch. Jana,[b] Xin-Yi Wang,[c] and Anangamohan Panja *[a,b]

[a] Department of Chemistry, Gokhale Memorial Girls' College, 1/1 Harish Mukherjee Road, Kolkata 700020, India

[b] Department of Chemistry, Panskura Banamali College, Panskura RS, WB 721152, India. E-mail: ampanja@yahoo.co.in

[c] State Key Laboratory of Coordination Chemistry, Collaborative Innovation Center of Advanced Microstructures, School of Chemistry and Chemical Engineering, Nanjing University, Nanjing, 210023, China. E-mail: wangxy66@nju.edu.cn

[d] Department of Chemistry, CICECO-Aveiro Institute of Materials, University of Aveiro, 3810-193 Aveiro, Portugal

Table of Contents

Fig. S1. ^{1}H NMR spectrum of ligand HL in $CDCl_3$ at indicated temperatures 4

Fig. S2. IR spectrum of ligand HL. 4

Scheme S1. Probable mechanism for the *in-situ* transformation of the Schiff base leading to the macrocyclic ligand. 5

Fig. S3. Electrospray ionization mass spectra (ESI-MS positive) of a reaction mixture related to the synthesis of $\mathbf{2_{Dy}}$ recorded after 5 min showing an important intermediate species (a) and the final product after 2 h (b) and (c). 5

Fig. S4. IR spectrum of $\mathbf{1}_{Gd}$ (ATR). 6

Fig. S5. IR spectrum of $\mathbf{2}_{Dy}$ (ATR). 6

Fig. S6. IR spectrum of $\mathbf{3}_{Gd}$ (ATR). 6

Fig. S7. IR spectrum of $\mathbf{4}_{Dy}$ (ATR). 7

Fig. S8. IR spectrum of $\mathbf{5}_{Gd}$ (ATR). 7

Fig. S9. IR spectrum of $\mathbf{6}_{Dy}$ (ATR). 7

Fig. S10. Ellipsoid plots of $\mathbf{1}_{Gd}$ - $\mathbf{6}_{Dy}$ with all sorts of solvent molecules and disorder models.....8

Fig. S11. SAPR coordination environment of complex $\mathbf{2_{Dy}}$ with the magic angle α between the S_8 axis and a Dy-L direction (left) and skew angle Φ between the diagonals of the two squares (right). 9

Fig. S12. Packing structure of $\mathbf{2_{Dy}}$ complex, viewed along the *b*-axis. Packing structure shows that the lattice contains a narrow 1-D pore channel along the *b*-axis. Molecules are shown in spacefill model. 9

Fig. S13. Packing structure of $\mathbf{2_{Dy}}$ complex, viewed along the b-axis. The pore channel is filled by disordered acetonitrile and water lattice solvent molecules, shown in spacefill model. Molecule is shown in capped stick model. 9

Fig. S14. Plots of $\chi_M T$ *versus T* under a 1000 Oe dc field in the temperature range of 2.0–300 K for three Gd complexes. Insert graph is Curie–Weiss analysis of the magnetic susceptibility data above 100 K with negative Weiss values. 10

Fig. S15 Plots of magnetization (M) versus magnetic field (H) at 2.0, 3.0 and 5.0 K in the field range of 0–7 T for three Gd complexes. 11

Fig. S16 Plots of magnetization (*M*) *versus* magnetic field (*H*) at 2.0 K in the field range of 0–7 T for three Dy complexes. 11

Fig. S17 Cole–Cole plots for $\mathbf{2_{Dy}}$ (a) and $\mathbf{6_{Dy}}$ (b) under 0 Oe dc field. The solid lines are the best fits to the experiments with the generalized Debye model. Arrhenius plot with the ln(τ) vs. T^{-1} for for $\mathbf{2_{Dy}}$ (c) and $\mathbf{6_{Dy}}$ (d). Red lines show fits of the data to the Arrhenius law $\tau = \tau_0 \cdot \exp(U\text{eff}/k\text{B}T)$, assuming the Orbach relaxation process. Blue lines represent fits to all the data considering other possible processes as indicated. 11

Fig. S18 Cole–Cole plots for $\mathbf{4_{Dy}}$ under zero dc field (a) and at 1000 Oe dc field (b). The solid lines are the best fits to the experiments with the generalized Debye model. 12

Fig. S19 (a) Frequency dependence and (b) temperature dependence of the in-phase and out-of-phase parts of the ac magnetic susceptibilities for $\mathbf{4_{Dy}}$ collected at 1000 Oe dc field at 2.0 K to 15.0 K. 12

Fig. 20. Ground state magnetic anisotropy of complexes $\mathbf{2}_{Dy}$ (a), $\mathbf{4}_{Dy}$ (b) and $\mathbf{6}_{Dy}$ (c). The Green rods represent the orientations of the anisotropy axes for each of the Dy^{III} ion in these complexes calculated by Magellan programme. 13

Table S1. Crystallographic data and refinement parameters of the complexes 14

Table S2. SHAPE analysis of the Ln^{III} ion in complexes $\mathbf{1}_{Gd}$–$\mathbf{6}_{Dy}$. 15

Table S3 Relaxation fitting parameters from the least-square fitting of the Cole-Cole plots of $\mathbf{2}_{Dy}$ under a 0 Oe dc field at 2.0-8.5 K according to the generalized Debye model. 15

Table S4 Relaxation fitting parameters from the least-square fitting of the Cole-Cole plots of $\mathbf{4}_{Dy}$ under a 0 Oe dc field at 2.0-8.5 K according to the generalized Debye model. 16

Table S5 Relaxation fitting parameters from the least-square fitting of the Cole-Cole plots of $\mathbf{4}_{Dy}$ under a 1000 Oe dc field at 2.0-8.5 K according to the generalized Debye model. 17

Table S6 Relaxation fitting parameters from the least-square fitting of the Cole-Cole plots of $\mathbf{6}_{Dy}$ under a zero Oe dc field at 2.0-8.5 K according to the generalized Debye model. 17

Table S7 Parameters fitted from the Arrhenius relationship for $\mathbf{2}_{Dy}$, $\mathbf{4}_{Dy}$ and $\mathbf{6}_{Dy}$ considering only the Orbach process. 18

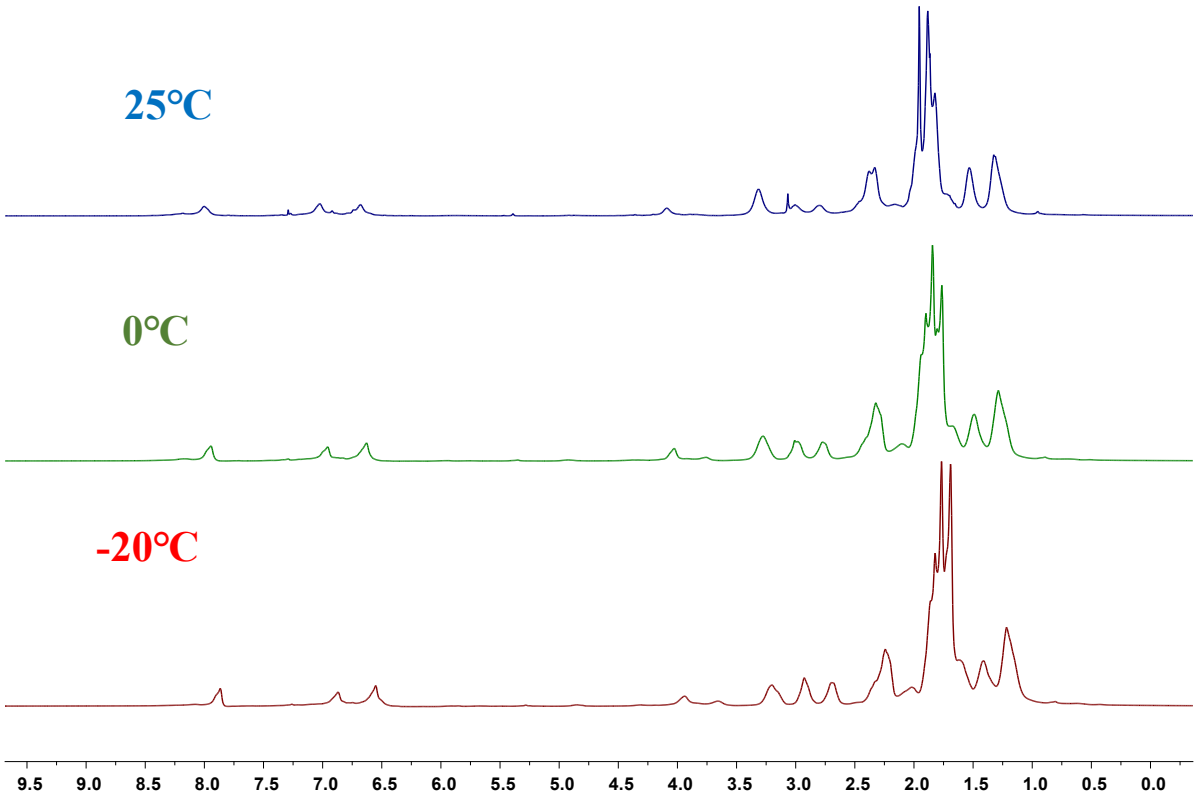

Fig. S1. ^{1}H NMR spectrum of ligand HL in $CDCl_3$ at indicated temperatures

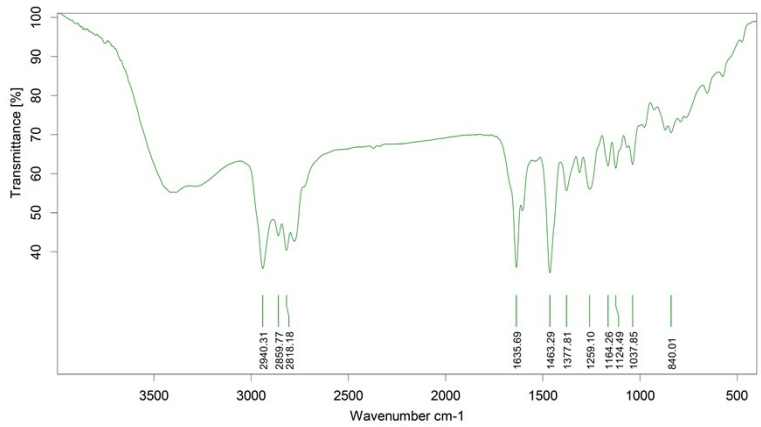

Fig. S2. IR spectrum of ligand HL.

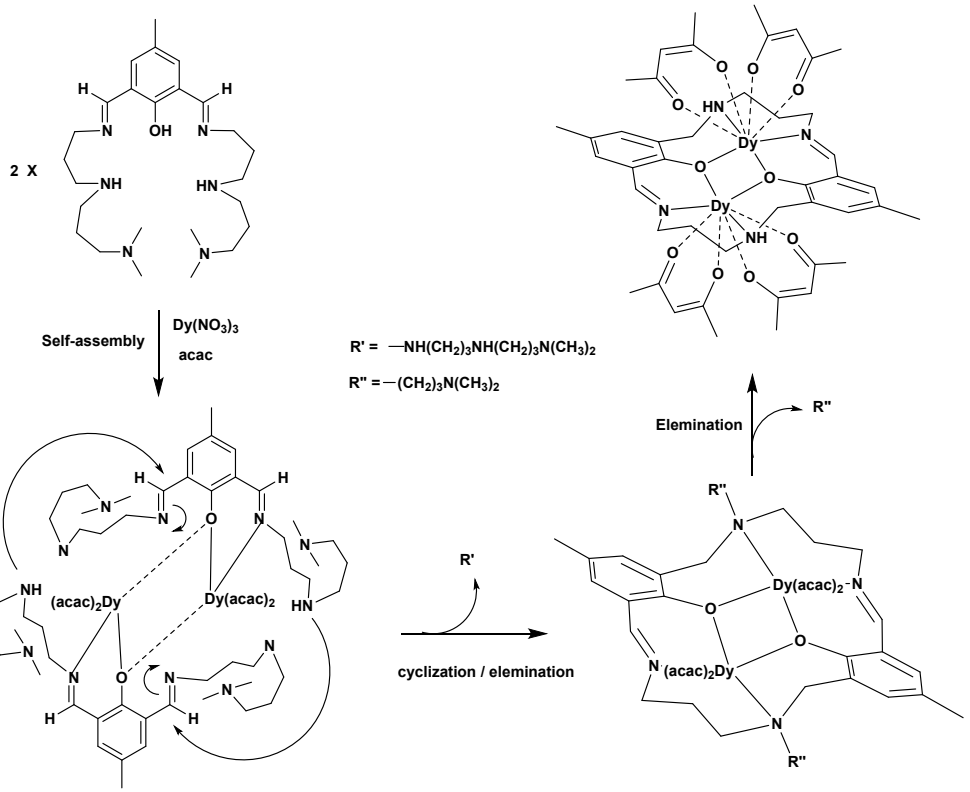

Scheme S1. Probable mechanism for the *in-situ* transformation of the Schiff base leading to the macrocyclic ligand.

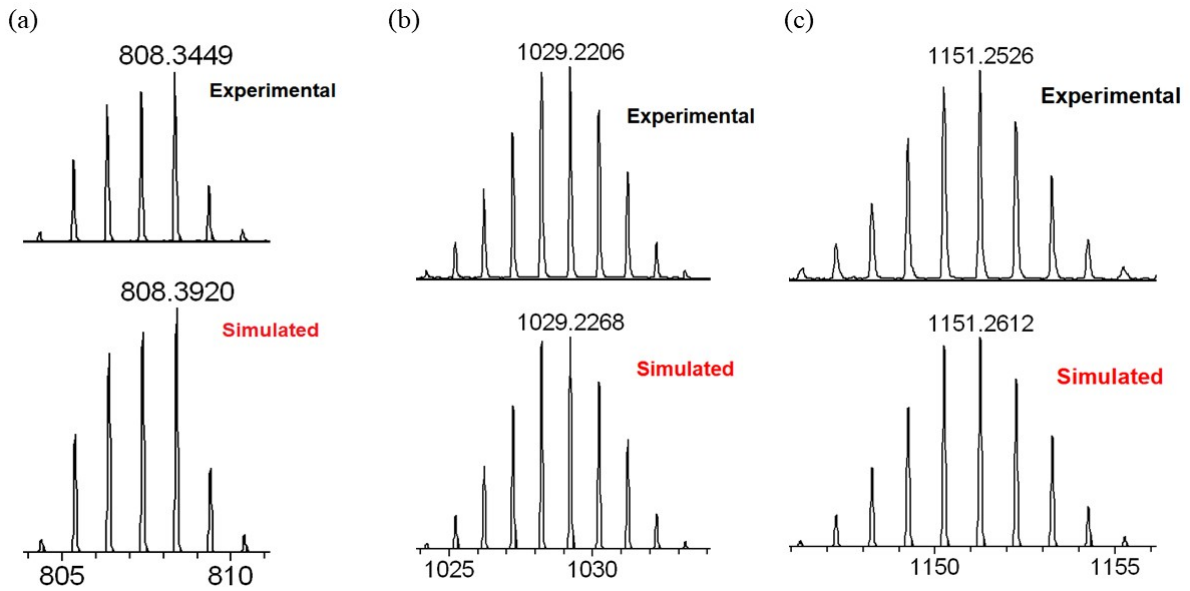

Fig. S3. Electrospray ionization mass spectra (ESI-MS positive) of a reaction mixture related to the synthesis of $\mathbf{2}_{\mathbf{Dy}}$ recorded after 5 min showing an important intermediate species (a) and the final product after 2 h (b) and (c).

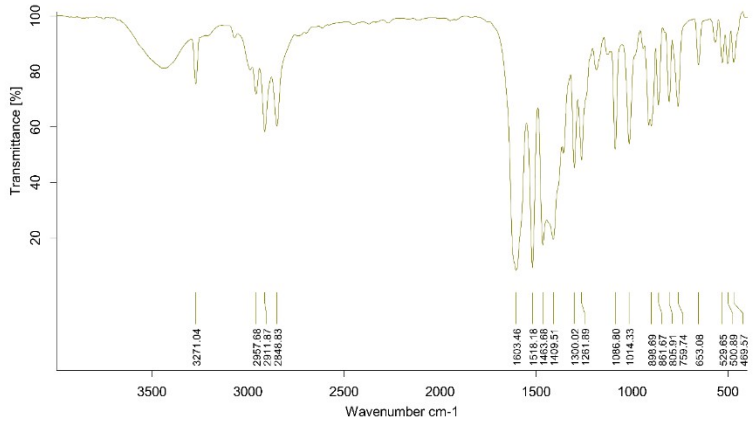

Fig. S4. IR spectrum of $\mathbf{1}_{Gd}$ (ATR).

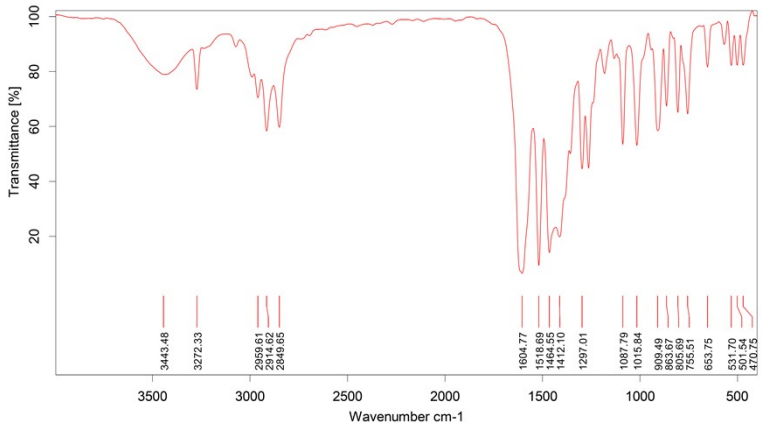

Fig. S5. IR spectrum of $\mathbf{2}_{Dy}$ (ATR).

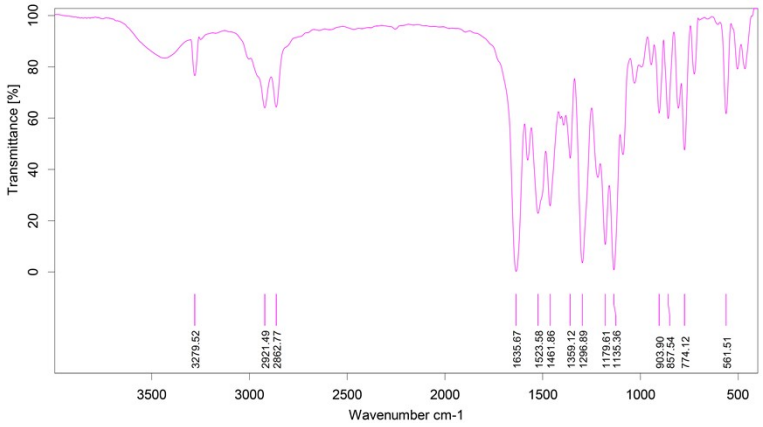

Fig. S6. IR spectrum of $\mathbf{3}_{Gd}$ (ATR).

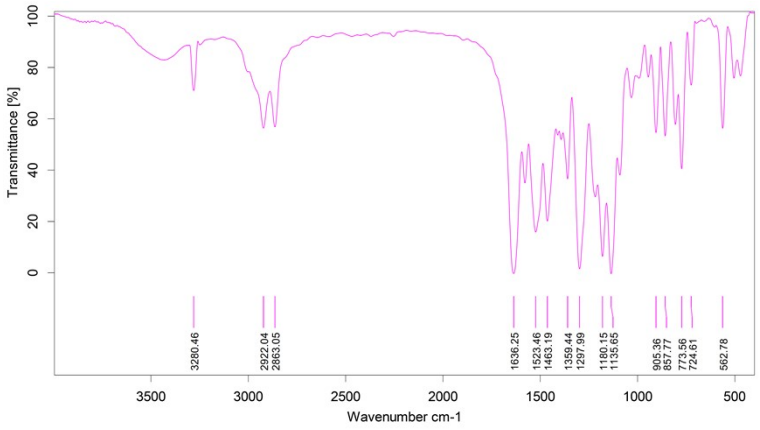

Fig. S7. IR spectrum of $\mathbf{4}_{Dy}$ (ATR).

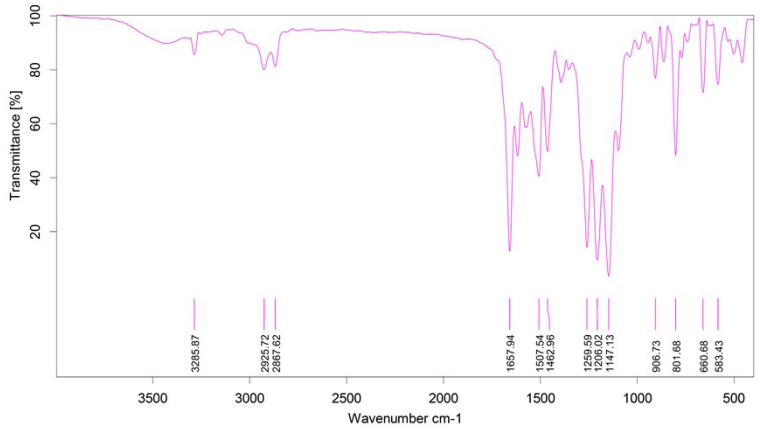

Fig. S8. IR spectrum of $\mathbf{5}_{Gd}$ (ATR).

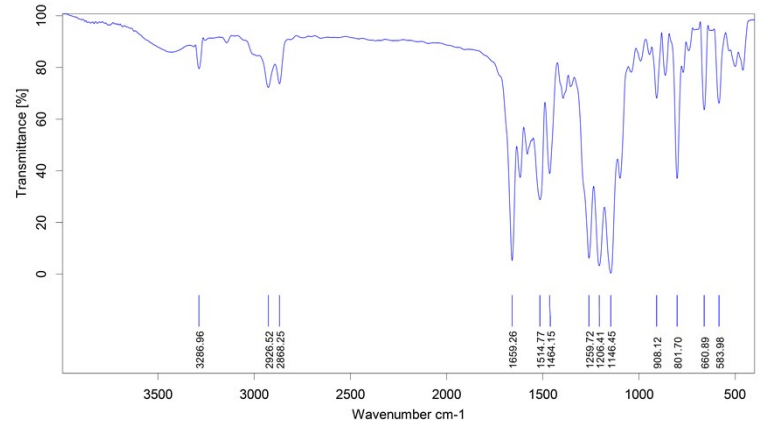

Fig. S9. IR spectrum of $\mathbf{6}_{Dy}$ (ATR).

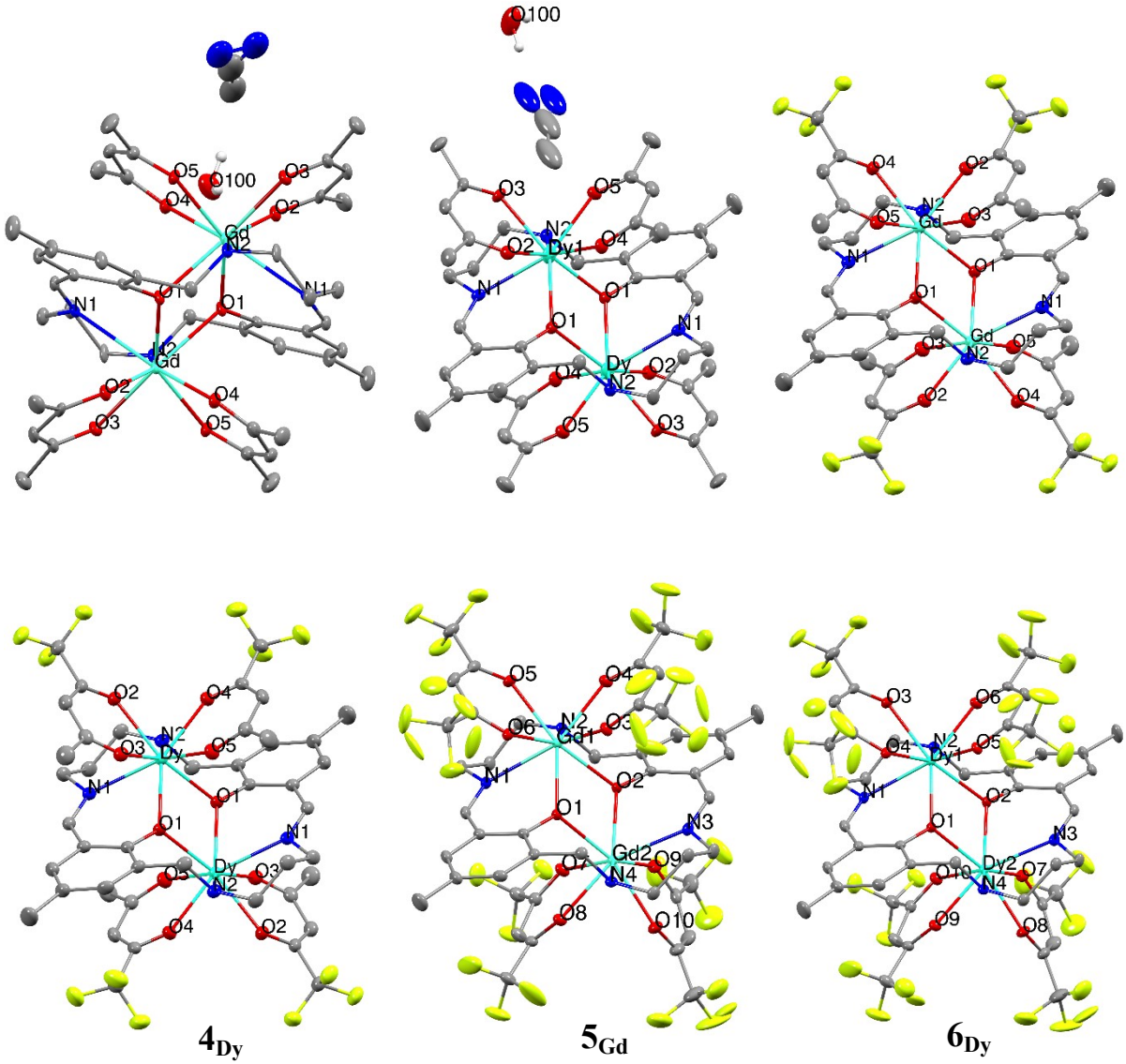

Fig. S10. Ellipsoid plots (30 % probability) of $\mathbf{1}_{Gd}$ - $\mathbf{6}_{Dy}$ with all sorts of solvent molecules and disorder models

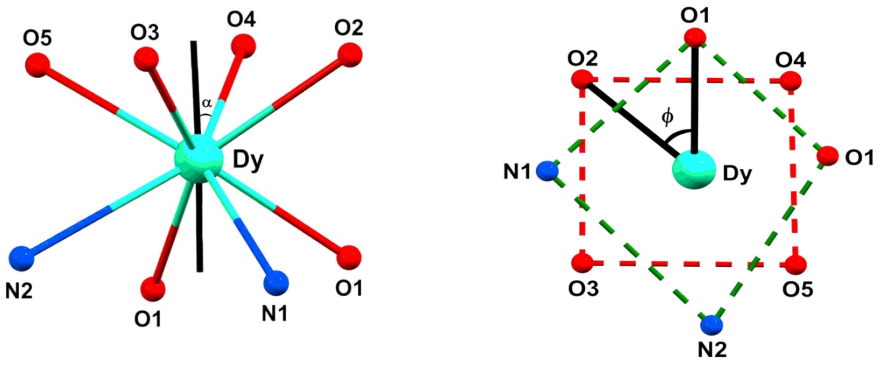

Fig. S11. SAPR coordination environment of complex $\mathbf{2_{Dy}}$ with the magic angle α between the S_8 axis and a Dy-L direction (left) and skew angle Φ between the diagonals of the two squares (right).

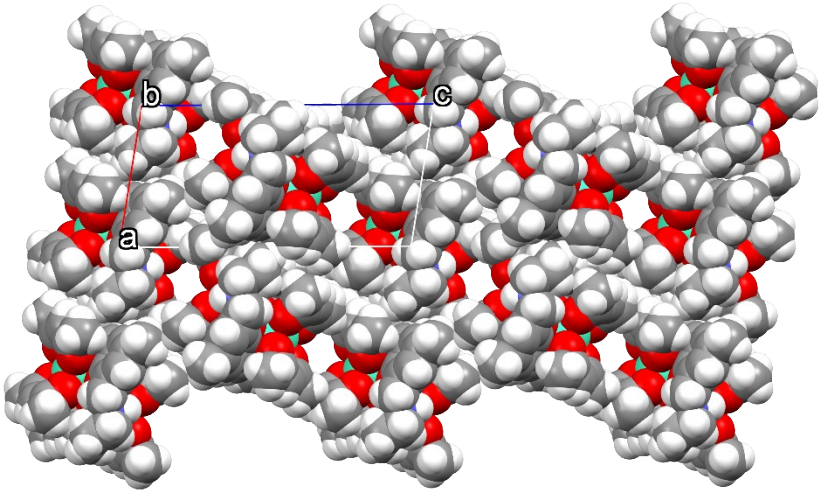

Fig. 12. Packing structure of $\mathbf{2_{Dy}}$ complex, viewed along the *b*-axis. Packing structure shows that the lattice contains a narrow 1-D pore channel along the *b*-axis. Molecules are shown in spacefill model.

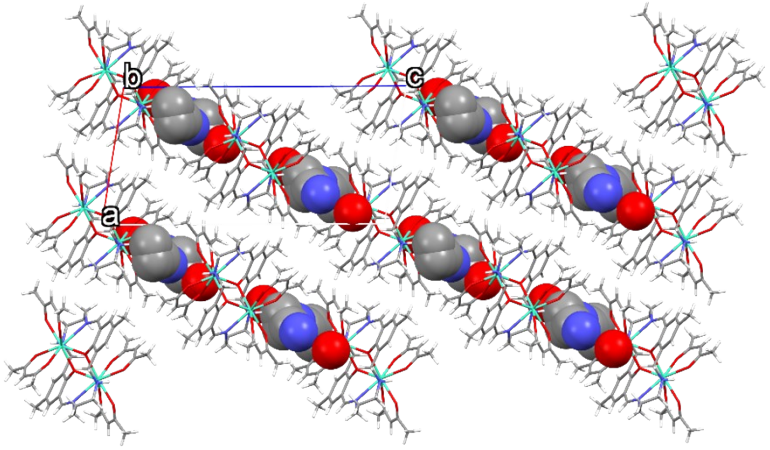

Fig. 13. Packing structure of $\mathbf{2_{Dy}}$ complex, viewed along the b-axis. The pore channel is filled by disordered acetonitrile and water lattice solvent molecules, shown in spacefill model. Molecule is shown in capped stick model.

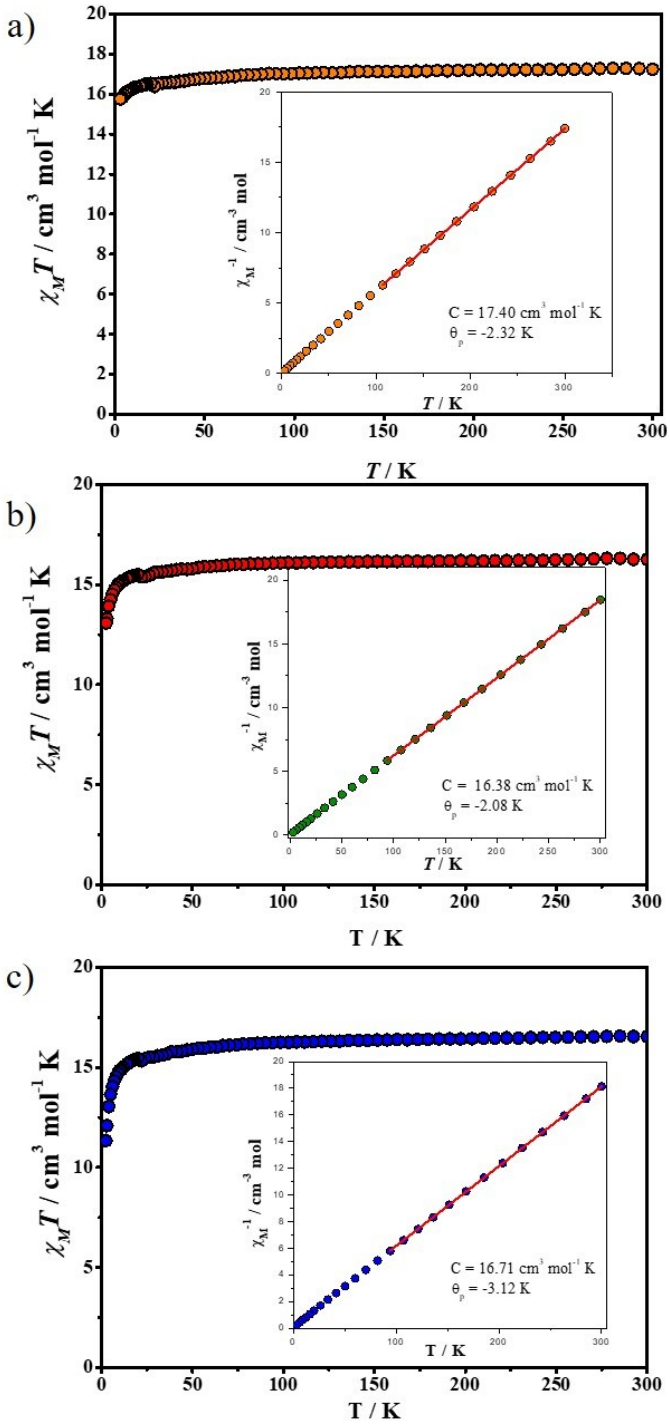

Fig. S14. (a)-(c) Plots of $\chi_M T$ *versus* T under a 1000 Oe dc field in the temperature range of 2.0–300 K for three Gd complexes $\mathbf{1}_{Gd}$, $\mathbf{3}_{Gd}$ and $\mathbf{5}_{Gd}$, respectively. Insert graph is Curie–Weiss analysis of the magnetic susceptibility data above 100 K with negative Weiss values.

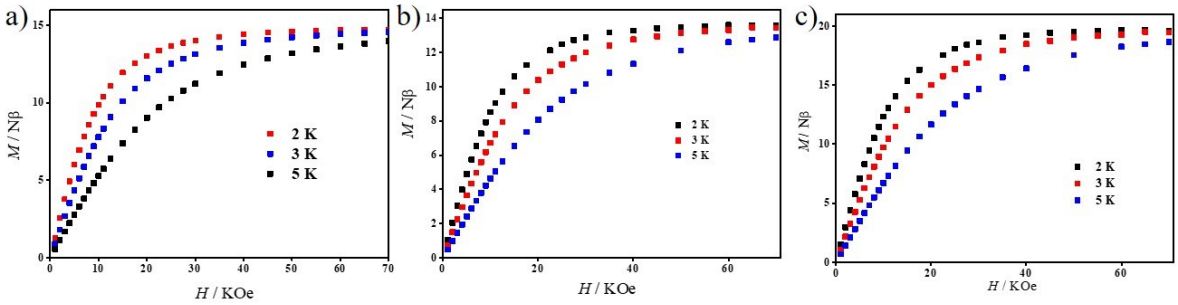

Fig. S15 Plots of magnetization (M) versus magnetic field (H) at 2.0, 3.0 and 5.0 K in the field range of 0–7 T for three Gd complexes.

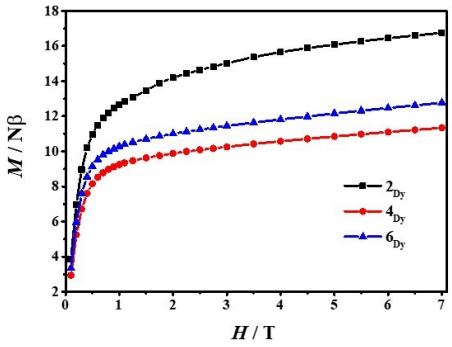

Fig. S16 Plots of magnetization (*M*) *versus* magnetic field (*H*) at 2.0 K in the field range of 0–7 T for three Dy complexes.

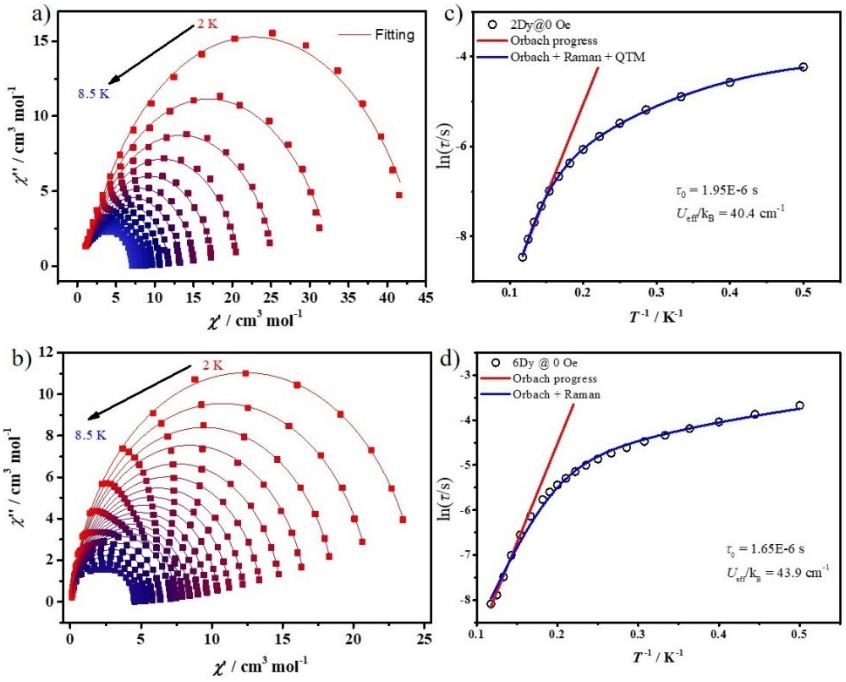

Fig. S17 Cole–Cole plots for $\mathbf{2_{Dy}}$ (a) and $\mathbf{6_{Dy}}$ (b) under 0 Oe dc field. The solid lines are the best fits to the experiments with the generalized Debye model. Arrhenius plot with the ln(τ) vs. T^{-1} for for $\mathbf{2_{Dy}}$ (c) and $\mathbf{6_{Dy}}$ (d). Red lines show fits of the data to the Arrhenius law $\tau = \tau_0 \cdot \exp(U\text{eff}/k\text{B}T)$, assuming the Orbach relaxation process. Blue lines represent fits to all the data considering other possible processes as indicated.

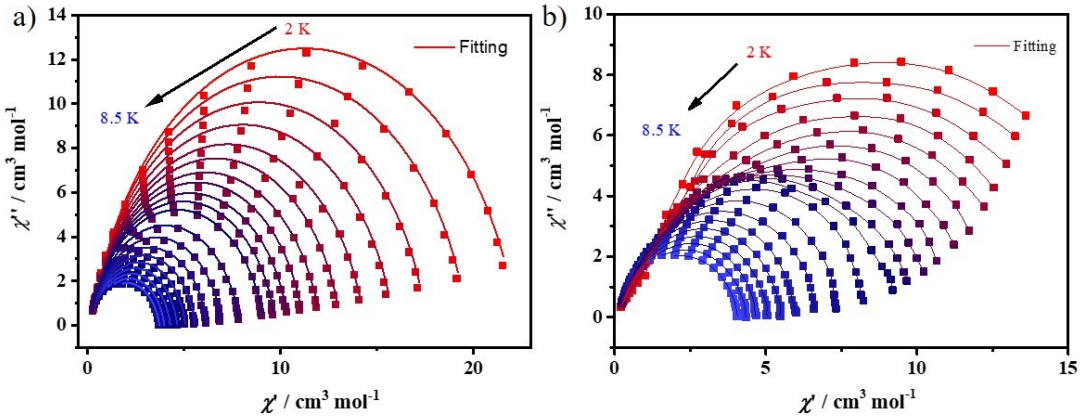

Fig. S18 Cole–Cole plots for $\mathbf{4_{Dy}}$ under zero dc field (a) and at 1000 Oe dc field (b). The solid lines are the best fits to the experiments with the generalized Debye model.

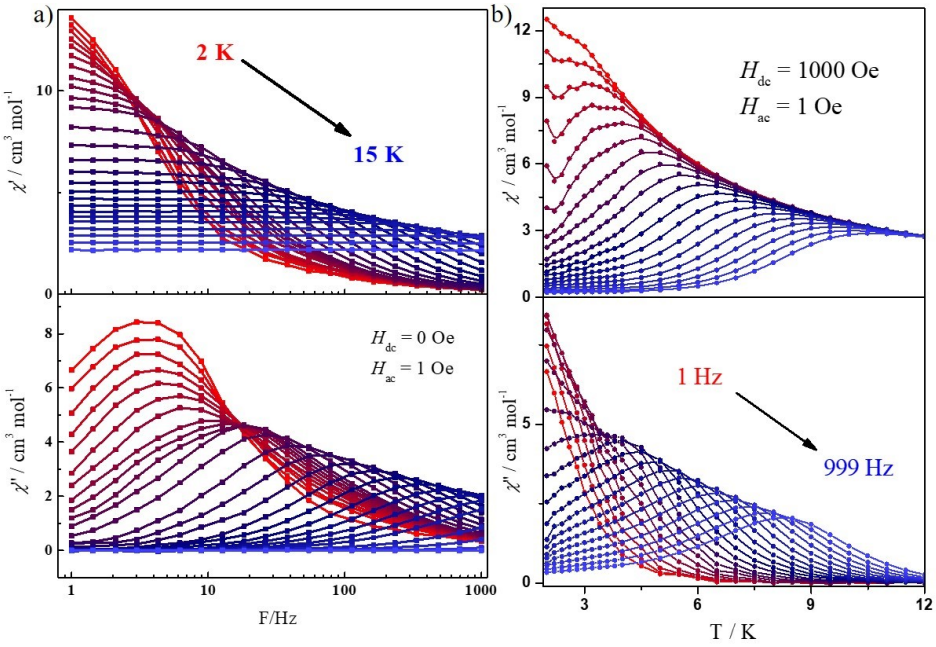

Fig. S19 (a) Frequency dependence and (b) temperature dependence of the in-phase and out-of-phase parts of the ac magnetic susceptibilities for $\mathbf{4_{Dy}}$ collected at 1000 Oe dc field at 2.0 K to 15.0 K.

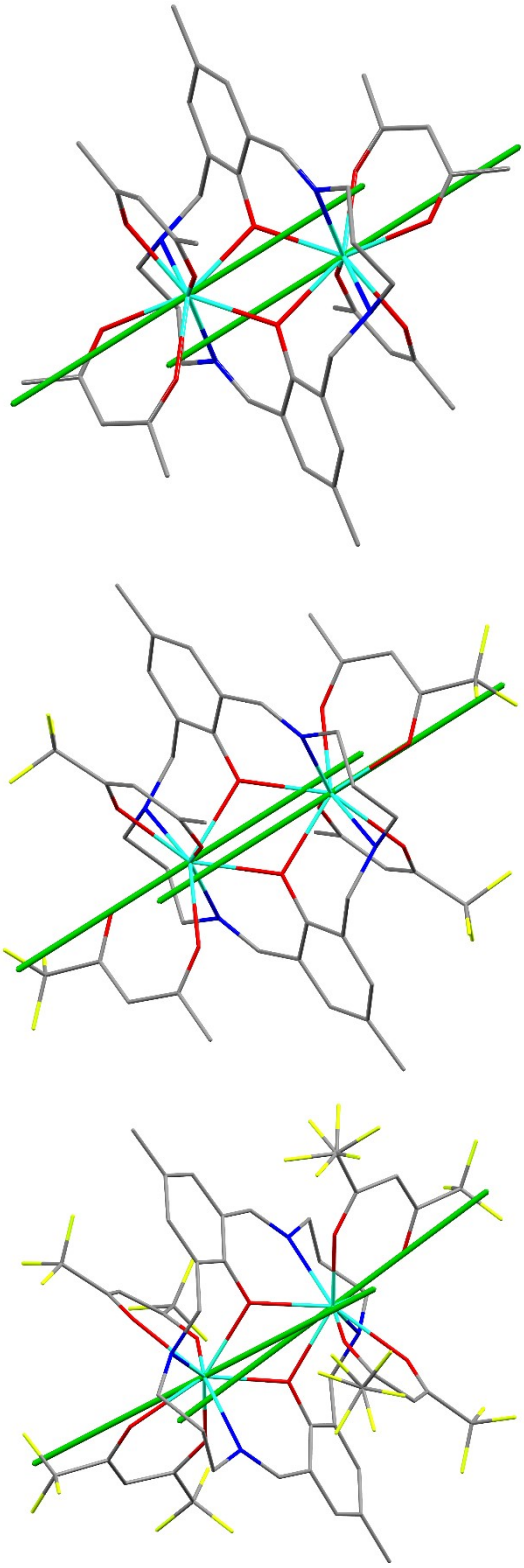

Fig. 20. Ground state magnetic anisotropy of complexes $\mathbf{2_{Dy}}$ (a), $\mathbf{4_{Dy}}$ (b) and $\mathbf{6_{Dy}}$ (c). The Green rods represent the orientations of the anisotropy axes for each of the Dy^{III} ion in these complexes calculated by Magellan programme.

Table S1. Crystallographic data and refinement parameters of the complexes

	$\mathbf{1}_{Gd}$	$\mathbf{2}_{Dy}$	$\mathbf{3}_{Gd}$	$\mathbf{4}_{Dy}$	$\mathbf{5}_{Gd}$	$\mathbf{6}_{Dy}$
CCDC No.						
Empirical formula	$C_{48}H_{66}Gd_2N_6O_{11}$	$C_{48}H_{66}Dy_2N_6O_{11}$	$C_{44}H_{46}Gd_2N_4O_{10}F_{12}$	$C_{44}H_{46}Dy_2N_4O_{10}F_{12}$	$C_{44}H_{34}Gd_2N_4O_{10}F_{24}$	$C_{44}H_{34}Dy_2N_4O_{10}F_{24}$
Formula weight	1217.56	1228.06	1333.35	1343.85	1549.25	1559.75
Crystal system	monoclinic	monoclinic	monoclinic	monoclinic	monoclinic	monoclinic
Space group	$P2_1/n$	$P2_1/n$	$P2_1/n$	$P2_1/n$	$P2_1/c$	$P2_1/c$
a/Å	10.9193(5)	10.8976(5)	12.3866(5)	12.3307(4)	17.5215(5)	17.4671(7)
b/Å	10.7257(6)	10.7327(5)	15.8527(7)	15.7913(5)	15.8691(4)	15.8149(6)
c/Å	22.1996(11)	22.0512(10)	12.3961(5)	12.3988(4)	19.1889(5)	19.2355(8)
β/°	99.344(4)	99.464(3)	98.654(2)	99.045(2)	91.384(2)	91.169(2)
Volume/Å^3	2565.5(2)	2544.0(2)	2406.40(17)	2384.25(13)	5333.9(2)	5312.5(4)
Z	2	2	2	2	4	4
ρ_{calc}g/cm^3	1.576	1.603	1.840	1.872	1.929	1.950
μ/mm^{-1}	2.625	2.977	2.839	3.217	2.607	2.934
F(000)	1224	1232	1308	1316	3000	3016
Θ range/°	1.859 to 27.138	1.873 to 27.190	2.100 to 29.181	2.105 to 27.182	1.162 to 29.192	1.166 to 29.190
Reflections collected	16870	5922	34099	34008	93576	80677
Independent reflections	5615 [R_{int} = 0.0591]	5922 [R_{int} =0.0731]	6500 [R_{int} = 0.0608]	5250 [R_{int} = 0.0492]	14424 [R_{int} =0.0567]	14323 [R_{int} =0.0538]
Data/restraints/parameters	4114/3/303	4968/8/310	4645/0/332	4336/1/332	11070/20/832	11194/14/839
Goodness-of-fit on F^2	1.027	1.033	1.016	1.027	1.026	1.009
Final *R* indexes [I>=2σ (I)]	R_1 = 0.0462, wR_2 = 0.0965	R_1 = 0.0569, wR_2 = 0.1353	R_1 = 0.0353, wR_2 = 0.0670	R_1 = 0.0261, wR_2 = 0.0605	R_1 = 0.0323, wR_2 = 0.0560	R_1 = 0.0318, wR_2 = 0.0611
Final *R* indexes [all data]	R_1 = 0.0756, wR_2 = 0.1078	R_1 = 0.0709, wR_2 = 0.1465	R_1 = 0.0637, wR_2 = 0.0765	R_1 = 0.0367, wR_2 = 0.0660	R_1 = 0.0529, wR_2 = 0.0627	R_1 = 0.0497, wR_2 = 0.0680
Largest diff. peak/hole / e Å^{-3}	1.661/-1.257	3.498/-2.331	0.965/-0.676	0.790/-0.506	1.009/-0.739	1.273/-1.041

Table S2. SHAPE analysis of the Ln^{III} ion in complexes $\mathbf{1_{Dy}}$–$\mathbf{6_{Gd}}$.

Label	Shape	Symmetry	$\mathbf{1_{Gd}}$	$\mathbf{2_{Dy}}$	$\mathbf{3_{Gd}}$	$\mathbf{4_{Dy}}$	$\mathbf{5_{GD}}$		$\mathbf{6_{Dy}}$	
OP-8	Octagon	D_{8h}	30.367	30.201	30.126	29.910	30.196	30.015	30.011	30.650
HPY-8	Heptagonal pyramid	C_{7v}	22.803	23.090	23.010	23.138	22.350	22.993	22.494	23.100
HBPY-8	Hexagonal bipyramid	D_{6h}	15.495	15.624	15.162	15.343	15.459	14.856	15.612	15.122
CU-8	Cube	O_h	9.643	9.678	8.760	8.915	9.714	9.295	9.819	9.484
SAPR-8	Square antiprism	$\boldsymbol{D_{4d}}$	**1.015**	**0.976**	**0.908**	**0.866**	**0.880**	**1.079**	**0.842**	**1.023**
TDD-8	Triangular dodecahedron	D_{2d}	2.078	2.109	1.947	1.975	2.213	2.125	2.183	2.128
JGBF-8	Johnson gyrobifastigium J26	D_{2d}	14.811	14.873	15.127	15.216	15.049	14.189	15.112	14.327
JETBPY-8	Johnson elongated triangular bipyramid J14	C_{3h}	27.524	27.583	27.104	27.266	27.172	27.241	27.304	27.265
JBTPR-8	Biaugmented trigonal prism J50	C_{2v}	2.225	2.238	2.672	2.650	2.547	2.849	2.557	2.862
BTPR-8	Biaugmented trigonal prism	C_{2v}	1.729	1.809	2.146	2.167	2.031	2.071	2.079	2.056
JSD-8	Snub diphenoid J84	D_{2d}	4.490	4.515	5.075	5.020	4.500	4.376	4.470	4.381
TT-8	Triakis tetrahedron	T_d	10.436	10.470	9.598	9.749	10.543	10.092	10.630	10.271
ETBPY-8	Elongated trigonal bipyramid	D_{3h}	22.933	23.061	22.455	22.652	22.650	22.853	22.860	22.926

Table S3 Relaxation fitting parameters from the least-square fitting of the Cole-Cole plots of $\mathbf{2_{Dy}}$ under a 0 Oe dc field at 2.0-8.5 K according to the generalized Debye model.

T / K	χ_S / $cm^3mol^{-1}K$	χ_T / $cm^3mol^{-1}K$	τ / s	α
2.0	0.99350	44.52550	0.01459	0.21507
2.5	0.88434	32.97310	0.01036	0.22121
3.0	0.86286	25.87344	0.00751	0.21862
3.5	0.86035	21.17176	0.00561	0.21448
4.0	0.85785	17.78734	0.00416	0.20957
4.5	0.90351	15.33025	0.00311	0.19958
5.0	0.95815	13.45134	0.00232	0.18936
5.5	1.01975	11.91325	0.00171	0.17720
6.0	1.09496	10.75745	0.00127	0.16617
6.5	1.15327	9.73973	9.19901E-4	0.15600
7.0	1.24263	8.92938	6.58684E-4	0.14493
7.5	1.33613	8.21976	4.59592E-4	0.13488
8.0	1.42255	7.63612	3.14415E-4	0.12988
8.5	1.52758	7.11068	2.1121E-4	0.12180

Table S4 Relaxation fitting parameters from the least-square fitting of the Cole-Cole plots of $\mathbf{4_{Dy}}$ under a 0 Oe dc field at 2.0-8.5 K according to the generalized Debye model.

T / *K*	χ_S / $cm^3mol^{-1}K$	χ_T / $cm^3mol^{-1}K$	τ / s	α
2.0	0.22465	22.26788	0.01235	0.13306
2.2	0.23750	19.68974	0.01079	0.12182
2.4	0.22855	17.56987	0.00960	0.11826
2.6	0.19820	15.86716	0.00875	0.12104
2.8	0.18444	14.34189	0.00777	0.12163
3.0	0.19669	13.11307	0.00706	0.11535
3.2	0.17709	12.05449	0.00641	0.11755
3.4	0.19816	11.17365	0.00579	0.11066
3.6	0.16872	10.41820	0.00531	0.11634
3.8	0.17871	9.73975	0.00481	0.11346
4.0	0.16187	9.12499	0.00436	0.11633
4.5	0.16703	7.87638	0.00331	0.11367
5.0	0.17965	6.94075	0.00246	0.11149
5.5	0.19306	6.16914	0.00178	0.10897
6.0	0.20282	5.56782	0.00126	0.11136
6.5	0.23429	5.06509	8.85029E-4	0.10996
7.0	0.27348	4.63379	6.13115E-4	0.10812
7.5	0.30798	4.27560	4.23371E-4	0.11094
8.0	0.35831	3.96373	2.90294E-4	0.11202
8.5	0.38254	3.71027	1.96181E-4	0.12457

Table S5 Relaxation fitting parameters from the least-square fitting of the Cole-Cole plots of $\mathbf{4_{Dy}}$ under a 1000 Oe dc field at 2.0-8.5 K according to the generalized Debye model.

T / *K*	χ_S / $cm^3mol^{-1}K$	χ_T / $cm^3mol^{-1}K$	τ / s	α
2.0	4.13868E-14	22.2108	0.06957	0.23962
2.2	4.92233E-14	21.2496	0.06924	0.25628
2.4	9.437E-14	19.5193	0.05829	0.26395
2.6	1.34918E-13	18.0294	0.04624	0.27801
2.8	2.00018E-13	16.7949	0.03815	0.28976
3.0	3.85775E-13	14.9469	0.02771	0.26382
3.2	5.3708E-13	13.7376	0.02166	0.25916
3.4	8.9624E-13	12.5071	0.01641	0.25905
3.6	1.0281E-12	11.6786	0.01366	0.23823
3.8	1.59975E-12	10.8375	0.01093	0.21652
4.0	2.57318E-12	10.1279	0.00852	0.18941
4.5	4.74762E-12	8.88421	0.00541	0.15962
5.0	8.74319E-12	7.74808	0.00334	0.12681
5.5	1.45765E-11	6.90561	0.00214	0.11102
6.0	2.65448E-11	6.18039	0.00139	0.09756
6.5	5.31108E-11	5.63134	9.15526E-4	0.08231
7.0	8.80143E-11	5.15889	6.15776E-4	0.07493
7.5	1.41107E-10	4.74827	4.17905E-4	0.06527
8.0	2.23511E-10	4.39588	2.87853E-4	0.0571
8.5	4.34836E-10	1.08991	2.01024E-4	0.05218

Table S6 Relaxation fitting parameters from the least-square fitting of the Cole-Cole plots of $\mathbf{6_{Dy}}$ under a zero Oe dc field at 2.0-8.5 K according to the generalized Debye model.

T / *K*	χ_S / $cm^3mol^{-1}K$	χ_T / $cm^3mol^{-1}K$	τ / s	α
2.0	0.10135	24.62746	0.02541	0.06737
2.2	0.09377	21.37005	0.02086	0.0685
2.5	0.08631	18.80932	0.01759	0.06922
2.7	0.09556	16.72003	0.01517	0.06222
3.0	0.07358	15.0065	0.01306	0.07373
3.2	0.06987	13.57511	0.01138	0.07437
3.5	0.07205	12.36927	0.00994	0.07417
3.7	0.07786	11.37886	0.00877	0.07262
4.0	0.07995	10.52561	0.00772	0.07251
4.2	0.07607	9.73978	0.00671	0.07325
4.5	0.08428	9.08421	0.00584	0.07032
4.7	0.07982	8.47095	0.00502	0.07051
5.0	0.08878	7.98016	0.00434	0.06833
5.2	0.09149	7.53222	0.00371	0.06754
5.5	0.0811	7.11841	0.00314	0.07127
6.0	0.08639	6.39961	0.00216	0.07222
6.5	0.07563	5.82483	0.00413	0.08548
7.0	0.05691	5.34813	9.0612E-4	0.11209
7.5	0.0798	4.93755	5.61986E-4	0.14665
8.0	0.28165	4.58862	3.75357E-4	0.17324
8.5	0.8145	4.27318	3.079E-4	0.14959

Table S7 Parameters fitted from the Arrhenius relationship for $\mathbf{2_{Dy}}$, $\mathbf{4_{Dy}}$ and $\mathbf{6_{Dy}}$ considering only the Orbach process.

complexes	$\mathbf{2_{Dy}}$	$\mathbf{4_{Dy}}$		$\mathbf{6_{Dy}}$
dc field	0 Oe	0 Oe	1000 Oe	0 Oe
τ_0 /s	1.95E-6	1.61E-6	1.53E-6	1.65E-6
U_{eff} / K(cm^{-1})	58.1 (40.4)	59.9 (41.3)	60.11 (41.8)	63.13 (43.9)
R^2	0.9972	0.9916	0.9999	0.9940

Table S8 Parameters fitted for $\mathbf{2_{Dy}}$, $\mathbf{4_{Dy}}$ and $\mathbf{6_{Dy}}$ by considering multiple relaxation processes using $\frac{1}{\tau} = \tau_{QTM}^{-1} + CT^n + \frac{1}{\tau_0}e^{-\frac{U_{eff}}{T}}$ and $\frac{1}{\tau} = CT^n + \frac{1}{\tau_0}e^{-\frac{U_{eff}}{T}}$ for the zero-field and 1 kOe dc field data.

complexes	$\mathbf{2_{Dy}}$	$\mathbf{4_{Dy}}$		$\mathbf{6_{Dy}}$
dc field	0 Oe	0 Oe	1000 Oe	0 Oe
τ_0 /s	3.17E-7	1.68E-7	1.00E-7	3.64E-7
U_{eff} / K(cm^{-1})	60.1 (41.8)	61.5 (45.7)	60.0 (41.7)	63.13 (43.9)
C / s^{-1} K^{-n}	2.4	23.5	10	13.01
n	3.1	1.7	4.0	1.6
τ_{QTM}	1.40E-2	1.20E-2	-	-
R^2	0.9998	0.9992	0.9946	0.9949